Temperature and humidity within a mobile barchan sand dune, implications for microbial survival

Michel Yves Louge, Alexandre Valance, Ahmed Ould El Moctar, Jin Xu, Anthony G. Hay, Renee Richer

Temperature and humidity within a mobile barchan sand dune, implications for microbial survival

M. Y. Louge,[1] A. Valance,[2] A. Ould el-Moctar,[3] J. Xu,[1] A. G. Hay,[4] and R. Richer[5]

Received 25 April 2013; revised 26 October 2013; accepted 29 October 2013.

[1] Although microorganisms play an important role in biological soil crusts and plant rhizospheres in deserts, it is unclear whether temperature and moisture deep within relatively fast moving hyperarid mobile dunes present a suitable habitat for microbes. To inform this question, we report measurements of temperature and humidity from probes initially sunk below the leeward avalanche face of a mobile barchan dune in the Qatar desert, emerging windward after 15 months of deep burial. Despite large diurnal variations on the surface, temperature within this dune of 5.6 m height is predictable, as long as dune advection is properly considered. It evolves on smaller amplitude and longer timescale than the surface, lagging average seasonal atmospheric conditions by about 2 months. We contrast these deep thermal records with measurements of diurnal variations of the temperature profile just below the surface, which we calculate with a thermal model predicting the relative roles of wind-driven convective heat transfer and net radiation flux on the dune. Observations and analyses also suggest why random precipitation on the leeward face produces a more unpredictable moisture patchwork on the windward slope. By rapidly reaching sheltered depths, small quantities of rain falling on that face escape evaporation and endure within the dune until resurfacing upwind. At depths below 10 cm, we show that moisture, rather than temperature, determines the viability of microbes and we provide initial microscopic and respiration-based evidence of their presence below the windward slope.

Citation: Louge, M. Y., A. Valance, A. Ould el-Moctar, J. Xu, A. G. Hay, and R. Richer (2013), Temperature and humidity within a mobile barchan sand dune, implications for microbial survival, *J. Geophys. Res. Earth Surf.*, *118*, doi:10.1002/2013JF002839.

1. Introduction

[2] Moderate temperatures and sufficient humidity are essential geophysical prerequisites for microscopic life in hyperarid habitats. For example, moisture controls the physiological activity of nitrogen and carbon fixation in biological soil crusts (BSCs), which contain a mixture of cyanobacteria, lichens, mosses, fungi, and algae. BSCs are common on hard desert floors and play an important role in the ecosystem dynamics of dry land [*Bokhary*, 1998]. Conversely, once formed, BSCs affect hydrology, including infiltration and runoff, albeit in ways that remain poorly understood [*Belnap*, 2005].

[3] Surface moisture also affects aeolian processes, which govern the shape, speed, and direction of mobile dunes [*Zhang et al.*, 2010, 2012]. For instance, in spite of arid conditions, droplets condense at dawn when the surface temperature descends below the dew point [*Kidron et al.*, 2002], forming ephemeral liquid bridges among grains once water penetrates the sand bed [*Frank and Perré*, 2012]. Small amounts of liquid as low as 0.05% by mass can then increase grain cohesion [*Mason et al.*, 1999; *Tegzes et al.*, 2003; *Mitarai and Nori*, 2006], impeding aeolian erosion [*Ravi et al.*, 2006] but temporarily stiffening the sand surface, thus enhancing transport [*Ho et al.*, 2011; *Rotnicka*, 2013].

[4] Another example where moisture, life, and geophysics are intertwined is in the rhizosphere of desert plants. Where such plants grow, arbuscular mycorrhizae fungi enhance the acquisition of water and nutrients by the roots of the plant host, thus ensuring its survival and facilitating soil fixation [*Stutz et al.*, 2000; *Requena et al.*, 2001; *Titus et al.*, 2002].

[5] Recently, *Gommeaux et al.* [2010] and *Heulin et al.* [2003, 2012] showed that BSCs and plant rhizospheres

Additional supporting information may be found in the online version of this article.

[1]Sibley School of Mechanical and Aerospace Engineering, Cornell University, Ithaca, New York, USA.
[2]Institut de Physique de Rennes, CNRS UMR 6251, Université de Rennes 1, Rennes, France.
[3]Laboratoire de Thermocinétique, UMR CNRS 6607, Ecole Polytechnique de l'Université de Nantes, Nantes, France.
[4]Microbiology, Cornell University, Ithaca, New York, USA.
[5]Weill Cornell Medical College in Qatar, Qatar Foundation, Doha, Qatar.

Corresponding author: M. Y. Louge, Sibley School of Mechanical and Aerospace Engineering, Cornell University, Ithaca, NY 14853, USA. (MYL3@cornell.edu)

2169-9003/13/10.1002/2013JF002839

are not alone in harboring desert microbes. They found that stationary, nonvegetated desert sand dunes in southeast Morocco contained approximately a thousand culturable microbes for every gram of sand. These surprising observations prompted questions about the internal temperature and moisture that would allow these microorganisms to exist. If such favorable internal habitats could last long enough, the observations of *Gommeaux et al.* [2010] also raised the intriguing possibility that relatively rapid mobile desert dunes could also contain live microbes, even though the collective motion of their sands does not normally permit the establishment of BSCs or plants [*Fang et al.*, 2007] and relentless aeolian surface renewal works against the preservation of their moisture.

[6] In fact, as this article will show, microorganisms are found below the surface of crescent-shaped barchan dunes, even though the latter can turn over their entire sand mass much more rapidly than the dune studied by *Gommeaux et al.* [2010]. This presence was unexpected, since microbial viability is ultimately tied to sufficient sand moisture and moderate heat, whereas harsh atmospheric conditions, solar radiation, aeolian erosion of the windward slope, redeposition of dry sands on the leeward avalanche face, and rare precipitation all conspire against favorable humidity and temperature. Until this work, it was unclear how microbes could find suitable habitat in relatively fast moving hyperarid dunes.

[7] While much attention has been paid to the aeolian transport that forms desert dunes [*Livingstone et al.*, 2007], fewer studies have focused upon their interior, and none have recorded the moisture and temperature habitat deep below the surface. To our knowledge, there is no prior attempt to model or simulate the internal heat and mass transfer within a mobile object of such size. In addition, because the traveling velocity of a mobile dune is typically on the same order as the thermal diffusion speed through sand, it was hitherto unclear how this motion affects the internal temperature of the dune.

[8] Nonetheless, understanding the deep habitat of mobile dunes is crucial to ensure the success of stabilization strategies. The relentless encroachment of mobile dunes on infrastructure has prompted efforts to fix them through land use restrictions [*Levin et al.*, 2007], artificial fixing by wind barriers or checkerboards [*Fang et al.*, 2007], and restoration of disturbed BSCs [*Bowker et al.*, 2008]. Natural dune stabilization also involves other factors, including the release and oxidation of iron from primary minerals, known as rubification [*Ben-Dor et al.*, 2006], and the development of physical soils crusts by deposition of wind-borne salts, silts, and clays [*Fang et al.*, 2007]. In marine dunes, *Forster* [1979] found that microbes play an important stabilizing role, even before BSCs form. In such landforms, more frequently battered by rain than their desert counterparts, she observed how bacteria aggregate sand by secreting extracellular polysaccharides [*Hu et al.*, 2002, 2003]. The resulting sand cohesion thus reduces wind erosion and increases moisture and nutrient content [*Forster and Nicolson*, 1981].

[9] In general, stabilization of a mobile sand dune requires an ecological synergy between geophysics, meteorology, plant biology, zoology, and microbiology. Although the complex feedback underlying this synergy remains misunderstood, it depends crucially upon heat and moisture. If desert sand dunes travel too fast for plants to take root, or if moisture becomes depleted by extended drought, the stabilization process breaks down [*Durán and Herrmann*, 2006; *Yizhaq et al.*, 2007]. It might recover with favorable moisture and temperature, through competing mechanisms involving heat transfer, penetration of scarce rainwater and ambient water vapor, aeolian transport in the turbulent boundary layer, granular cohesion and friction, and granular flow on leeward faces.

[10] In short, heat and moisture are important geophysical attributes of mobile sand dunes. Focusing attention on these parameters, we show that barchans conceal regions of moderate temperature and sufficient humidity to permit the survival of microbes. Despite their mobility, barchan dunes preserve moisture acquired during infrequent rains. As they progress downwind, humidity adsorbed on sand grains immobilized under the leeward slope resurface at their toe, thus compensating for moisture lost to windward aeolian erosion.

[11] To expose such internal heat and moisture processes, we sunk probes with data storing and broadcasting capabilities through the avalanche slope of a barchan in Qatar. These instruments remained buried where they were trapped while the dune passed overhead, until they finally emerged windward several months later. To gauge how deeply dune sands could protect microbes from extreme environmental conditions, we also contrasted these observations with vertical temperature and humidity profiles acquired just below the surface. These profiles revealed that wide diurnal variations in solar radiation and atmospheric conditions only affect temperature and moisture to a relatively shallow depth, thus allowing the dune to shelter milder conditions in its midst on longer timescales. They also suggested that surface humidity at dawn can temporarily affect aeolian transport and sand cohesion.

[12] We begin with a geophysical description of mobile barchan dunes. We then present and interpret measurements of temperature and humidity just below the surface. We contrast these measurements with those of deeply buried probes and show that moisture adsorbed on sand grains can persist within the mobile dune for a long time. Finally, we present respiration data and microscopic observations as evidence of biological activity.

2. Mobile Barchan Dunes

[13] Mobile dunes pose insidious threats to human infrastructure. Their relatively slow but relentless wind-driven advance rarely brings them to the attention of civil or industrial planners. Attempts to stop them by planting *Prosopis* trees or erecting simple barriers are often unsuccessful [*Sterk*, 2003]. In general, wind-driven granular transport determines the morphology and shape of hyperarid deserts [*Bagnold*, 1935; *McKee*, 1979; *Zhang et al.*, 2010, 2012]. On the edge of a sand sea, barchan dunes like the one we studied (Figure 1) form where an inexhaustible sand supply meets a flat plain subject to a prevailing wind direction [*Livingstone et al.*, 2007]. Their crescent shape makes it possible to model the surrounding flow [*Schwämmle and Herrmann*, 2005] and to understand their behavior [*Rasmussen et al.*, 1996; *Sauermann et al.*, 2001; *Andreotti et al.*, 2002; *Hersen et al.*, 2004; *Ould Ahmedou et al.*, 2007].

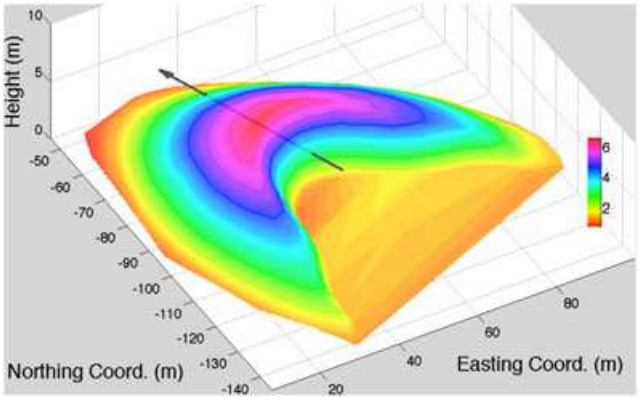

Figure 1. Shape of the Qatar dune under study on 16 July 2012. Easting, northing, and altitude refer to the datum on hard ground at 25°00′35.82″N, 51°20′24.54″E near the weather station. The arrow is the estimated path relative to the dune of probe 1, which disappeared below the surface on 1 May 2011. The leeward avalanche face is inclined at 31°, and the dune moves on an average bearing of 159°. Altitude is represented by the color scale shown and is exaggerated by a factor of $\simeq 3$.

[14] The gently rising windward face of a barchan is interrupted by a brink behind which air recirculates downward and inward. In its wake, suspended sand loses momentum and accumulates onto the steep leeward slope. Intermittent avalanches maintain this slope at its angle of repose by rapidly transferring excess grains downward. Sand involved in avalanches is trapped unless wind changes direction. Barchan dunes are thus mobile (Figure 2), with speed roughly in inverse proportion to their size [*Charru et al.*, 2013]. The lee face of the barchan dune is terminated by horns revealing the formation of "wing vortices" on either side and giving the dune its crescent shape. Sand escaping to the next barchan originates from these horns [*Hersen*, 2004].

[15] The barchan under study is outlined in Figure 1. It is part of a mobile dune field west of Mesaieed (Qatar) with speeds shown in Figure 2 and an average bearing of 160°. In Appendix E of the supporting information, we report positions of selected nearby dunes, as well as properties of their sands. Sand material density is $\rho_m \simeq 2630$ kg/m^3. Particle size distribution (PSD) varies within the dune. On the windward slope, its moments are $\bar{d} \simeq 351$ μm, $d_{20} \equiv (\overline{d^2})^{1/2} \simeq 365$ μm, and $d_{30} \equiv (\overline{d^3})^{1/3} \simeq 377$ μm, where the overbar denotes averaging over the PSD. Particles collected at the base of the leeward face are typically larger ($\bar{d} \simeq 346$ μm) than at the top ($\bar{d} \simeq 319$ μm), reflecting particle segregation in naturally intermittent granular avalanches [*Gray and Hutter*, 1997]. Such dense slides give rise to an inclined stratification featuring layers of larger particles ($\bar{d} \simeq 352$ μm, $d_{20} \simeq 365$ μm, and $d_{30} \simeq 376$ μm) interlaced with layers of smaller ones ($\bar{d} \simeq 312$ μm, $d_{20} \simeq 331$ μm, and $d_{30} \simeq 347$ μm). The pattern is buried as the dune moves forward, progressively reappearing on the upwind slope below the brink's elevation as rounded outlines of the old face.

[16] Until the observations of *Gommeaux et al.* [2010], it was unclear whether microbes could survive extreme conditions of a hyperarid, nonvegetated desert dune, as they do within biological soil crusts [*Belnap*, 2005] or the rhizosphere of desert plants [*Requena et al.*, 2001]. Intuition suggested that relatively fast moving mobile dunes would be less likely to shelter internal microbial activity. Informing this question required peering deep into the dune.

[17] Unfortunately, studies of the interior of sand dunes are rare. To investigate internal dune stratigraphy, *McKee* [1979] performed deep excavations and *Bristow et al.* [2000] used ground-penetrating radar. Recently, *Vriend et al.* [2012] used this technique to visualize cross strata in large dunes, and *Vriend et al.* [2007] investigated the acoustics of booming sands with seismic refraction. To elucidate the behavior of the "dry layer" near the surface of a desert dune, *Kobayashi et al.* [1986, 1991] measured temperature and humidity in the first 13 cm below the dune surface. During campaigns in the Negev desert, *Katata et al.* [2007] recorded incident radiation, derived latent heat flux from microlysimeter measurements below the dune surface, sand water content by gravimetric sampling, and turbulent transport flux of sensible heat with a sonic anemometer. *De Félice* [1968] recorded temperatures of the surface, at depths of 5 and 20 cm, and of ambient air 5 cm above. He also evaluated radiation fluxes at short and long wavelengths, which he reported for 1 h following solar noon. He then calculated a thermal diffusivity $\alpha_s \simeq 1.5\ 10^{-7}$ m^2/s for sand at his test site. *Chen* [2008] measured similar thermal conductivities for four quartz sands at various compactions and water volume fractions.

[18] As *Carslaw and Jaeger* [1959] showed, thermal diffusion penetrates the interior of a dune at a speed $u_d \equiv 2\sqrt{\alpha_s \pi/\tau}$, which is set by the period τ of thermal forcing at the surface. Therefore, over a year with $\tau = 365$ days, seasonal variations penetrate into our dry sands at a rate $u_d \simeq 12$ m/yr. As Figure 2 shows, because the mean dune speed U is comparable to u_d, the motion of the dune crucially affects its deep thermal response to seasonal variations. In contrast,

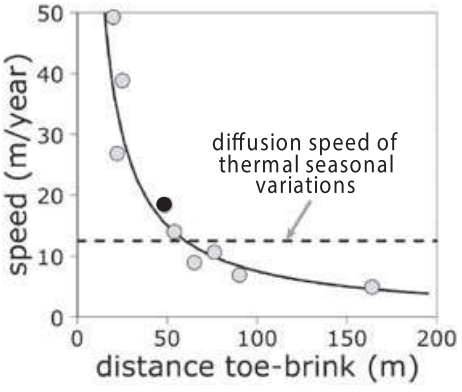

Figure 2. Dune speed U (m/yr) versus distance D (m) from windward toe to brink on the vertical plane of dune symmetry, derived from online historical images of Google Earth from October 2002 to September 2009 for the Qatar dune field studied (dune positions in Table F2). The line is the best fit $UD \simeq 750$ m^2/yr. The horizontal dashed line marks the diffusion speed $u_d = 2\sqrt{\alpha_s \pi/Y}$ of thermal seasonal variations on a timescale Y of a year. The filled circle represents the barchan under study.

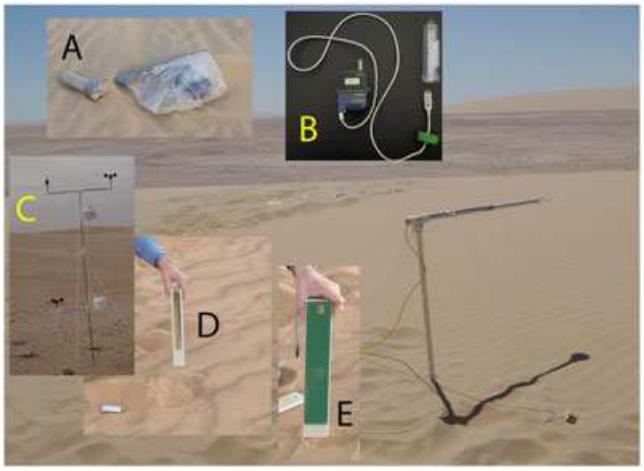

Figure 3. Instruments deployed. Background: radiometer at the tip of a Γ-shaped rod on the Qatar dune. (a) The probe described in section 4 resurfaces in July 2012. (b) Probe assembly: remotely controlled logger unit connected to the temperature/humidity sensor protected in a conical with ventilation holes. (c) Temporary weather station with two RH and *T* instruments, two anemometers, and a wind vane. (d) Fifteen sensor temperature probe and (e) capacitance probe about to be inserted through the dune surface.

thermal variations on the shorter diurnal timescale $\tau = 24$ h only penetrate a relatively shallow region below the surface. Because the corresponding diffusion speed $\simeq$ 240 m/yr far exceeds U, dune motion hardly matters to the diurnal thermal problem.

[19] In short, although prior work focused on diurnal thermal variations just below desert surfaces, little was known whether near-surface conditions allow microbial activity. Although dunes revealed a rich internal stratigraphy, the distribution of heat and moisture deep within fast-moving mobile dunes remained similarly unclear. To inform these questions, section 3 addresses conditions near the dune surface. Section 4 then considers heat and moisture deep within a mobile dune.

3. Near-Surface Diurnal Variations

[20] This section focuses upon diurnal variations of temperature and humidity just beneath the windward slope of the dune, toward establishing where microbes could be sheltered from hyperarid ambient conditions. To that end, we report data from two separate invasive probes recording temperature and adsorbed moisture. Unlike semiarid conditions investigated by *Katata et al.* [2007], our dune is drier, so that evaporation plays a minor role in the heat balance. We show that a thermal model incorporating wind-driven thermal convection and net radiation flux can capture temperature variations near the surface. Modern data acquisition allows us to report data in greater detail than *de Félice* [1968] and *Kobayashi et al.* [1986, 1991] and to produce a simultaneous animation of temperature depth profile, surface heat fluxes, and wind speed. By measuring thermal diffusivity of our sands in situ, these near-surface observations set the stage for deeper and longer measurements of temperature and humidity with the buried probes discussed in section 4.

3.1. Instruments

[21] On 19 March 2011, we deployed the two instruments on the windward toe of the mobile barchan sand dune in Figure 1 at 25°00′34.7″N, 51°20′24.9″E. The temperature probe consisted of a 305 mm long glass-filled Delrin lance of 41 mm width and 11 mm thickness, with a 10° taper to facilitate insertion into dune sands (Figure 3). Its long flat face was hollowed to lodge a Plexiglas housing of 227 mm × 24 mm × 9 mm protecting 15 LM235 National Semiconductor temperature sensors and their associated wires and resistors, all bound by epoxy resin into the assembly. Housing material and bonding were chosen to match the thermal diffusivity of bulk sand, in an effort to minimize thermal disruption by the probe.

[22] The robust temperature sensors were packaged in a small cylindrical capsule of 4.8 mm diameter that determines their vertical spatial resolution. They operated as two-terminal Zener diodes with breakdown voltage proportional to absolute temperature. We supplied their cathode with $\sim$ 10 V through a 12 kΩ resistor, connected anode to ground and recorded the breakdown voltage from cathode to ground. Although these sensors were meant to output 10 mV/°K, we calibrated each of them in the laboratory against a known ambient temperature. Once buried in sand, the sensors provided temperature at 15 independent depths x in the range $5 \leqslant x \leqslant 218$ mm from the free surface.

[23] We recorded the net radiation flux with a Kipp & Zonen "NR Lite 2" radiometer at 80 cm above the dune near the location where the temperature probe was buried. This robust instrument, shaped as a disk of 80 mm diameter, possessed a single component sensor that recorded the difference in a wide spectrum of wavelengths $0.2 < \lambda < 100$ μm between the net flux received from below (sand albedo and emission) on a circular absorbing patch of 34 mm diameter and the corresponding flux striking a similar patch from above (solar flux and atmospheric emission). Because the calibrated instrument sensitivity was relatively low ($12.5\ 10^{-6}$ V m^2/W), we boosted the output voltage with an amplifier of 100 gain before data acquisition.

[24] Signals from the temperature, moisture, and radiometer were multiplexed to a National Instrument cRIO data acquisition chassis with a real-time microcomputer controlling the data stream to and from a field programmable gate array. When powered with long-term lithium polymer batteries (or with lead acid batteries recharged by a 100 W solar panel), the chassis was autonomous, selecting each channel in turn for measurement. We buried it away from the probe location under a reflective "survival blanket" to avoid extreme conditions that might damage its electronics.

[25] Meanwhile, we erected a weather station on hard ground approximately 28 m upwind of the dune. It measured wind speed at elevations of $z_1 \simeq 0.9$ m and $z_2 \simeq 2.4$ m using two Second Wind "C3" three-cup magnetic induction anemometers producing an output frequency linear upon wind speed u, with detection threshold $\simeq$ 0.35 m/s. We also recorded wind direction at 2.4 m with a NRG #200P potentiometer wind vane, as well as ambient temperature T_z at $z \simeq 0.9$ m and $\simeq$ 2 m using two ThermoWorks TW-USB-2-LCD+ autonomous loggers with accuracy $T_z = \pm 0.3°C$, protected from direct and reflected solar radiation by open white plastic shields. A Second Wind "Nomad" data

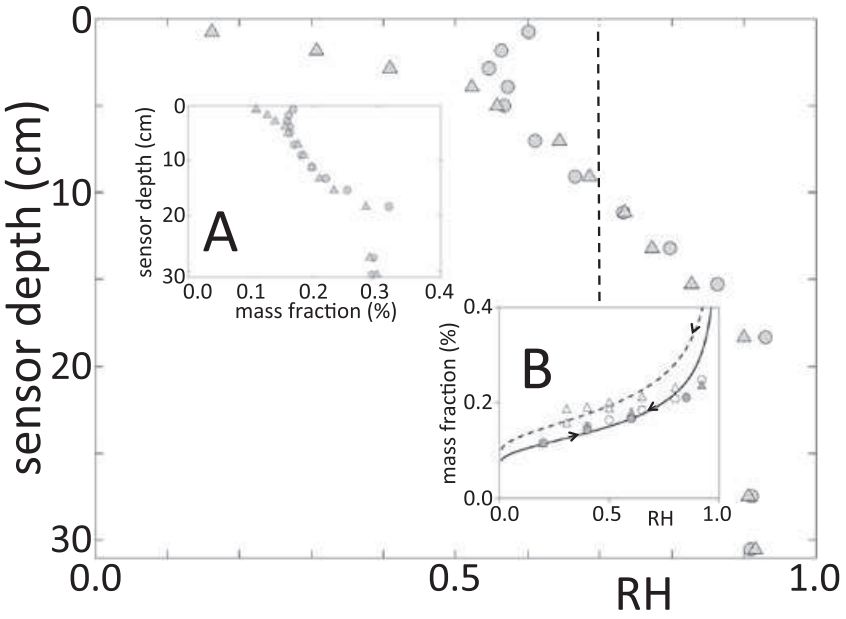

Figure 4. Depth profiles of relative humidity recorded at sunrise (circles) and as the sun culminated at solar noon (triangles) on 20 March 2011, inferred from equation (1) from the "loss tangent" of a 15 sensor variant of the capacitance probe of *Louge et al.* [2010]. In this case, microbial survival was likely inhibited at depths < 11 cm, where RH = a_w < 0.7 [*Mugnier and Jung*, 1985] (left of vertical dashed line) but probably not below. (a) Profiles of mass fraction Ω inferred from equation (3). Diurnal moisture variations only affected the first 5 cm and gradually rose with depth. (b) Isotherm data (symbols) and their corresponding fits to equation (3) (lines). In this inset, circles and triangles denote, respectively, the adsorption isotherm at increasing RH and its desorption counterpart at decreasing RH. At 40°C (filled symbols), the two isotherms nearly coincide and are fitted to $\Omega_\ell \simeq 0.0013$ (solid line). As expected from the relative insensitivity of ℓ_w on T in equation (2), the adsorption isotherm at 22°C (open circles) conforms to the same fit. However, desorption at 22°C (open triangles) lies above adsorption (open circles) and is fitted to $\Omega_\ell \simeq 0.0017$ (dashed line). In inset A, mass fraction Ω was converted to water activity with $\Omega_\ell \simeq 0.0015$ intermediate between the two values of Ω_ℓ.

logger acquired wind speed, direction, and temperature. All variables were recorded at 1 min intervals.

3.2. Moisture

[26] To record moisture profiles near the surface (Figure 4), we also deployed a probe similar to the one that *Louge et al.* [2010] used on a Mauritanian sand dune but possessing 15 sensors with spatial resolution of ∼ 3 mm in the vertical direction. Those authors provided an exhaustive description of the instrument. Its electronics produce a "loss tangent" $|\tan\varphi|$ that is correlated with the relative humidity in equilibrium with the surrounding sand grains. To find the correlation, we exposed samples of Qatar dune sand to a climate-controlled chamber at relative humidities in the range 0.30 < RH < 0.82 at 35°C. (The highest relative humidity (RH) is the upper stability limit of the electronics for this sand.) We found

$$|\tan\varphi| \simeq |\tan\varphi_0|[\exp(\mathrm{RH}/\mathrm{RH}_0) - 1], \tag{1}$$

where $\varphi_0 = 0.0241 \pm 0.0045$ rad and $\mathrm{RH}_0 = 0.233 \pm 0.013$. Using the same chamber operated at 0.3 < RH < 0.9 with temperatures of 22 and 40°C, we also related RH to the local fraction Ω of water mass adsorbed on sand grains relative to total sand mass by comparing weights of dry and moist samples. At our relatively low moisture levels, we followed *Shahraeeni and Or* [2010] in assuming that water storage was dominated by film adsorption on a thickness

$$\ell_w = \left[\frac{M_w A}{6\pi\rho_w \hat{R} T \ln(\mathrm{RH})}\right]^{1/3}, \tag{2}$$

where M_w is the molecular weight of water, ρ_w is its liquid density, $A < 0$ is Hamaker's constant, and $\hat{R}$ is the fundamental gas constant [*Iwamatsu and Horii*, 1996]. This relation implies the following dependence of relative humidity and mass fraction:

$$\mathrm{RH} = \exp[-(\Omega_\ell/\Omega)^3]. \tag{3}$$

[27] As inset B in Figure 4 shows, data at relatively low moisture levels conformed to equation (3) despite limited hysteretic behavior between water adsorption and desorption at 22°C similar to what *Shang et al.* [1995] observed.

[28] Figure 4 shows two profiles of relative humidity recorded on 20 March 2011 through a depth of 30.5 cm. At sunrise, dew briefly collected on the surface, raising the relative humidity to 60% there. Such level likely affected the erosion behavior of the sand surface, at least temporarily. For instance, *Fraysse et al.* [1999] observed rising values of the maximum angle of stability for a granular pile with RH $\gtrsim$ 0.4. Similarly, *Ravi et al.* [2006] reported from wind tunnel tests that the aeolian shear velocity threshold

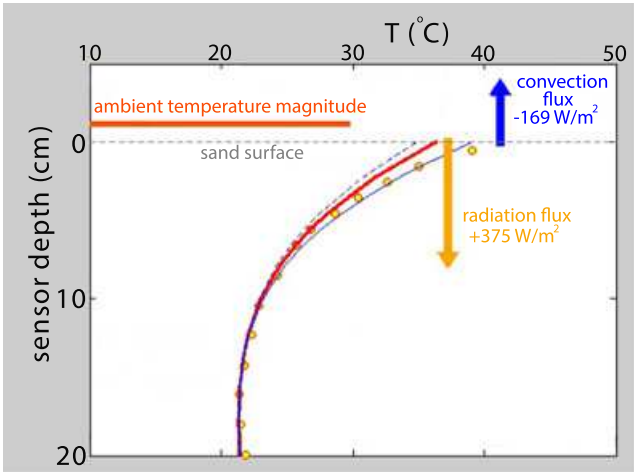

Figure 5. Typical temperature profile snapshot through the first 20 cm below the sand surface (horizontal dashed line) recorded at 11:09 A.M. Qatar time (UT+3h) on 21 March 2011 with an instantaneous wind speed of 4.5 m/s. The ordinate is depth in cm, and the abscissa is temperature in °C. The thick horizontal orange line shows ambient temperature T_z on that scale recorded at $z = z_T = 2$ m. Circles represent measurements, with symbol size equal to actual sensor diameter. The thick red line is the prediction of the thermal model with $\zeta \equiv u^*/u = 0.084$, $k_s = 0.49$W/m.°K, $\rho c_p = 1170$ J/m^3.°K, $\alpha_s = 3.9\ 10^{-7}$ m^2/s, $\epsilon_a = 0.7$, $\epsilon = 0.86$, $\omega = 0.64$, and the depth boundary condition $T_s \to 295$°K as $x \to \infty$. The dashed and solid blue lines are, respectively, $\zeta = 0.084 + 0.059$ and $0.084 - 0.059$ corresponding to its range of uncertainty. The left and right vertical arrows indicate measured net radiation and calculated thermal convection fluxes, respectively, counted positive into the dune. An animation of this figure from 19 to 21 March 2011 is available in the supporting information.

undergoes a transition within $0.4 \lesssim$ RH $\lesssim 0.65$. As the sun later reached solar noon, humidity nearly vanished at the surface, thus exposing the latter to unbridled aeolian erosion.

[29] Crucially, diurnal ambient humidity variations only affected the first 5 cm. Relative humidity then gradually increased with depth x, reaching a nearly constant level at $x \gtrsim 20$ cm. We will discuss what this profile implies for microbiology in section 5.

3.3. Thermal Model

[30] Figure 5 and its animation available online show temperature profiles recorded with the 15 sensor probe in the first 22 cm from the surface. As *de Félice* [1968] and *Kobayashi et al.* [1986, 1991] had already observed, harsh diurnal temperature variations were attenuated within a short distance $\sim$ 10 cm from the surface. To analyze this, we modeled subsurface thermal conditions in response to solar radiation and to convection by surface winds. The model assumed that sand has uniform heat diffusivity $\alpha_s = k_s/(\rho_s c_s)$, conductivity k_s, bulk density ρ_s, and specific heat per mass c_s. Because local moisture typically represents $<$ 0.3% of total sand mass anywhere near the surface, the model ignored latent heat release or variations of k_s with water content [*Chen*, 2008]. It also neglected radiative transfer within the porous sand which, according to the analysis of *Taine et al.* [2010], produces an effective radiation conductivity $< 2\ 10^{-3}\ k_s$. The conservation equation for sensible heat is then

$$\frac{\partial T_s}{\partial t} = \alpha_s \frac{\partial^2 T_s}{\partial x^2}, \tag{4}$$

where T_s is sand temperature in equilibrium with its surroundings and x is the downward vertical along the probe. At the free surface, continuity of the thermal flux imposes the boundary condition

$$-k_s \frac{\partial T_s}{\partial x} = \dot{q}''_{\text{rad}} + \dot{q}''_{\text{wind}}, \tag{5}$$

where $\dot{q}''_{\text{rad}}$ and $\dot{q}''_{\text{wind}}$ are, respectively, the net radiation and turbulent thermal fluxes received by the dune (positive downward).

[31] The supporting information in Appendices A ("Radiation Model") and B ("Thermal Boundary Layer") provides detailed calculations of these fluxes, so equation (4) may be solved numerically. However, it is instructive to recall first the simpler solution of a harmonic forcing of the surface temperature [*Carslaw and Jaeger*, 1959], which captures well the increasing time lag $x\sqrt{J/(4\pi\alpha_s)}$ of the peak temperature at depth x,

$$T_s = \bar{T}_{s0} + \Delta T_s \exp\left[-x\sqrt{\frac{\pi}{\alpha_s J}}\right] \sin\left[\frac{2\pi}{J}\left(t - \frac{J}{4}\right) - x\sqrt{\frac{\pi}{\alpha_s J}}\right], \tag{6}$$

where J is the diurnal period (24h), $\bar{T}_{s0}$ is the corresponding mean surface temperature, ΔT_s is total diurnal temperature excursion at the surface, and t is time from midnight, roughly halfway between sunset and sunrise. Following *de Félice* [1968], we used equation (6) to infer a bulk thermal diffusivity $\alpha_s \simeq 3.9\ 10^{-7}$ m^2/s for our sands from records of temperature peak time versus depth. Equation (6) also predicts that surface temperature variations decay exponentionally on a scale $x_J = \sqrt{\alpha_s J/\pi}$. In our experiments, $x_J \simeq 104$ mm, which justifies the design length of the temperature probe.

[32] Because the sky was free of clouds in these experiments, we estimated broadband radiative properties of our sands from the net flux collected by the differential radiometer. At night, the instrument recorded the difference between a relatively small atmospheric emission from above and infrared emission from the sand surface. This difference was mainly a measure of sand surface emissivity. During the day, it was struck above by solar radiation and atmospheric emission and by reflected light from the sand surface below. As outlined in Appendix A, knowledge of the dune surface temperature time-history and the clear-sky solar flux $\dot{q}''_{\text{sun}} \simeq 1353$ W/m^2 then yielded estimates of sand albedo $\omega \simeq 0.64$ and emissivity $\epsilon \simeq 0.86$ by least squares fitting the net radiometer signal over the entire experiment. We then used these quantities to predict the net radiative surface flux from solar ephemeris, taking into account local dune slant. (At the probe location, the skyward unit normal $\hat{\mathbf{n}}_d$ to the dune had an angular elevation of 77° and a bearing of 300°).

[33] Unfortunately, equation (6) was too crude to represent temperature variations driven by the complicated diurnal thermal flux through the sand surface. Instead, as detailed in Appendix B, we modeled the wind-generated

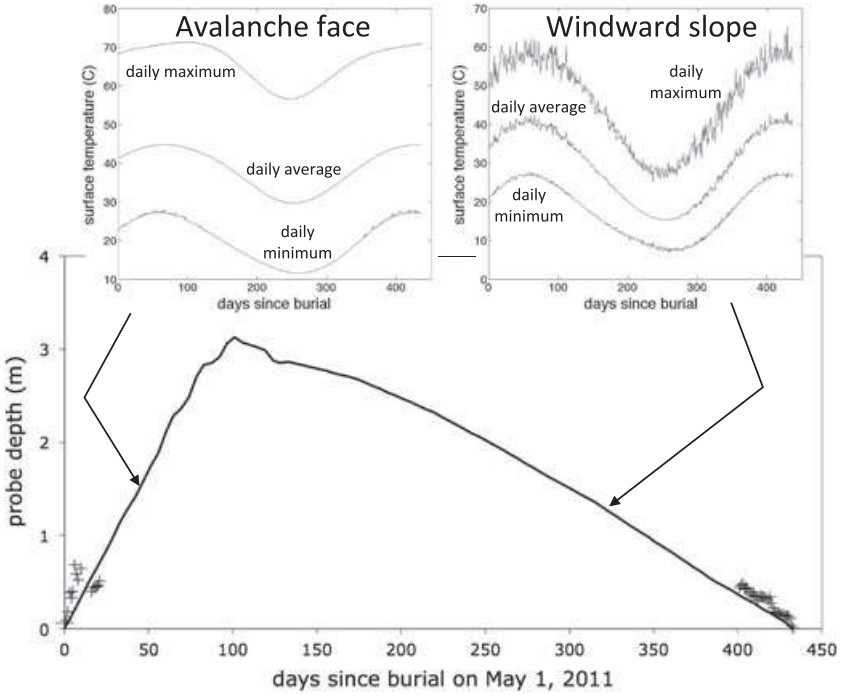

Figure 6. Bottom: vertical height of the sand column above probe 1 (line) estimated from the dune profile of Figure 1, and a uniform dune speed $U \simeq 26.2$ m/yr calculated from overall distance traveled and duration between burial and emergence. Such speed is 35% greater than the historical average 18.4 m/yr visible on Google Earth. Symbols are probe depth, inferred from recognizable time lags between solar noon and peak recorded temperature. Days are counted from 30 April 2011 until 6 July 2012. Top: daily minimum, average, and maximum sand surface temperatures calculated as outlined in Appendix D for the leeward avalanche face, assuming no convection (left); and for the windward slope with convection coefficient $\rho c_p \kappa \bar{\zeta} \bar{U}_m / \ln(z_T/\bar{\zeta}_0) \simeq 18$ W/m^2.°K.

convective contribution to the flux by invoking the Monin-Obukhov similarity [*Wyngaard*, 2010]. To find the overall surface flux boundary condition, we then added the net radiative flux calculated in Appendix A. Finally, we integrated partial differential equation (4) using the *pdepe* toolbox of Matlab, subject to $T_s = 295$°K at the distance $x = 5x_J$ deep into the dune.

[34] As Figure 5 shows, this thermal model captures temperature data well. To illustrate its ability to do so over two diurnal periods, we also provide an animation of the temperature profile for 19–21 March 2011. This movie reveals that equations (4) and (5) produce accurate predictions, particularly at night, when the dune surface, colder than the air aloft, created a stably stratified atmospheric boundary layer. The stabilization started approximately an hour before sunset, as the net radiation flux turned negative. The magnitude of the dune's radiation loss then reached a maximum and slowly decreased as surface temperature cooled. The net radiation flux turned positive about an hour after sunrise, rapidly inverting the temperature gradient at the surface and producing an unstably stratified thermal boundary layer with warmer sand than ambient air. Around solar noon, the model overestimated the calculated convective flux, yielding a surface temperature $\sim$ 5°C too low at that time. This discrepancy, perhaps due to our choice of parameters in the Monin-Obukhov similarity, underlines the importance of wind-driven thermal convection, which increased with wind speed, but was either directed into or out of the dune depending on the difference between ambient air and sand surface temperatures. In future experiments, one should record atmospheric profiles of fluctuating wind speed and temperature, so accuracy of the Monin-Obukhov similarity could be refined in this arid situation.

[35] Finally, it is interesting to note that, according to our calculations, the dune hardly experienced any heat gain or loss over the 24 h period from the first sunrise to the next. During that time, the integrated net radiation input was +4.62 10^6 J/m^2, while the integrated convective loss was –4.77 10^6 J/m^2, which represented a net loss of < 3% of the radiation input. Therefore, this patch of dune was nearly in thermal equilibrium with its ambient surroundings over the duration of this experiment in mid-March. In particular, the recorded mean diurnal ambient temperature was 22.4°C, an almost identical value to our predicted mean surface temperature of 23.0°C. (Meanwhile, the recorded excursion in ambient temperature was $14.1 < T_z < 31.6$°C, and our prediction of surface temperature spanned $13.2 < T_{s_0} < 35.8$°C.) However, as the next section suggests, such equilibrium of the surface flux does not persist over the whole year and/or on the entire dune.

4. Deeply Self-Buried Probes

[36] In this section, we report signals from self-buried probes confirming that temperature and humidity deep within the dune are unaffected by ambient diurnal variations.

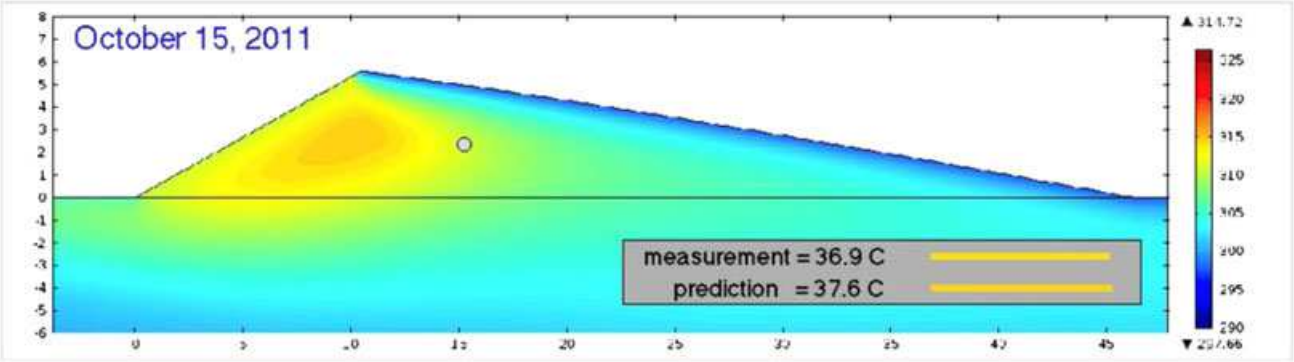

Figure 7. Two-dimensional simulation of equation (7) on the vertical dune cross section where the buried probe resided (gray circle). The interior color scheme indicates sand temperature in degrees kelvin. Distances are expressed in meter. The inset compares temperatures measured by the buried probe and the corresponding model predictions in degrees Celsius. The supporting information includes an animation of this figure.

We show that, although deep temperature can be accurately inferred from solar ephemeris and statistics on wind strength, deep humidity is more unpredictable, as it is sensitive to the random timing of rainfall, subsequent nonlinear water penetration, and dune motion.

4.1. Instruments

[37] As Figure 2 illustrated, the Qatar dunes establish an average forward speed that is inversely proportional to their length between toe and brink. We exploited this motion to investigate conditions deep beneath the surface by sinking two identical ThermoWorks TR-3310 temperature and humidity probes through the leeward avalanche face, waiting for the dune to overcome them. These instruments measured relative humidity RH $\pm$ 2% in the range 5% < RH < 95% and temperature $T_s \pm 0.3$°C in $0 < T_s < 55$°C. Each probe was attached to a RTR-53 recording unit that included a two-year battery, an antenna that allowed hand-held electronics to interrogate it remotely, and enough memory to record autonomously for 333 days. We protected them in a plastic container featuring several holes allowing humidity to pass while securing them against small animals burrowing through the avalanche face. We programmed them to acquire data each hour and interrogated them from time to time through sands as thick as 3 m. For a few days after burial and before emergence, we could infer probe depth x from our knowledge of sand thermal diffusivity α_s and the lag $x\sqrt{J/(4\pi\alpha_s)}$ predicted by equation (6) from solar noon to the time of peak recorded temperature. However, for days in between, temperature oscillations were too small to infer depths > 0.7 m in that way.

[38] Probe 1 was first buried on 26 March 2011 at 12:50 Qatar time (09:50 universal time). The avalanche covered it progressively, but it resurfaced and slid about halfway down the incline. It remained there until 1 May 2011, when it finally disappeared as the dune overcame it. The probe and its recording unit resurfaced unscathed on 6 July 2012. Probe 2 remained below the surface from its burial on 18 November 2011 at 16:15 Qatar time until it emerged in March 2013.

[39] Figure 1 shows a survey of the dune carried out on 16 July 2012 with a Leica TS-02 theodolite with extended-range (> 1000 m) electronic distance meter. With this instrument, we recorded precisely where probe 1 had emerged a few days earlier. Although the dune changed shape and tack somewhat between April 2011 and July 2012, we estimate that it migrated at constant speed above the immobilized probe 1, such that the latter appeared to "travel" on the reverse path shown as an arrow in Figure 1 relative to the dune. Assuming a uniform dune speed calculated from overall distance traveled and duration between burial and emergence, we then estimated probe depth shown in Figure 6.

4.2. Temperature

[40] Once buried deeply, the probes experienced relatively mild temperatures with seasonal variations smaller than diurnal oscillations. To predict them, we developed the two-dimensional thermal model of the dune's interior that is summarized in Appendix D ("Thermal Advection-Diffusion Deep Within a Mobile Dune"). Crucially, this model modifies the thermal equation (4) to include the dune velocity **U** explicitly,

$$\frac{\partial T_s}{\partial t} + \mathbf{U} \cdot \nabla T_s = \alpha_s \nabla^2 T_s. \tag{7}$$

Although we did not record the net surface radiation flux over the entire burial period, the sky was generally clear enough to estimate $\dot{q}''_{\mathrm{rad}}$ from solar ephemeris and radiation parameters provided in Appendix A. To evaluate the surface convection flux, we first noted that wind speed data from the weather station could be described as a random variable with reproducible diurnal variations and a peak with log normal distribution, described in Appendix C ("Ambient Temperature and Wind"). This allowed us to estimate $\dot{q}''_{\mathrm{wind}}$ with a Monte Carlo technique, and by integrating equation (4) in a "diurnal boundary layer" below the dune surface (Appendix D), we find the long time variations of daily mean surface temperature $\bar{T}_{s0}$ (Figure 6, top). We then used $\bar{T}_{s0}$ as an external boundary condition for 2-D integration of equation (7), which captures dune mobility through the constant advection speed **U**. As Figure 7 and its animation in the supporting information illustrate, such advection is crucial to the long timescales that are characteristic of the dune's interior.

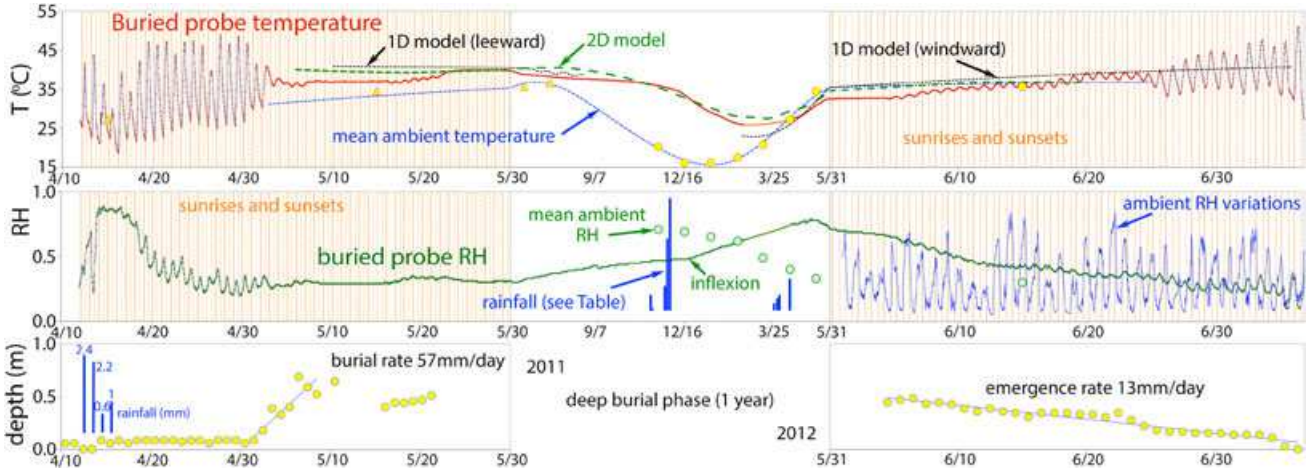

Figure 8. Data from probe 1 buried from April 2011 to July 2012. Top: three panes show buried temperature versus time. Timescales are magnified during burial and emergence phases to illustrate near-surface temperature oscillations similar to those discussed in section 3. Small red circles are individual buried temperature measurements at 1 h intervals; they merge into a thick red line as diurnal fluctuations attenuate. Vertical solid orange and dashed lines mark sunrises and sunsets, respectively. Data from 2 February 2012 to 14 April 2012 are interpolated from adjacent records when memory overflowed. The dashed blue line is the periodic fit (equation (C1)) of monthly averaged ambient temperatures measured on our weather station (circles) for 12 months from November 2011. (Triangles are extrapolations from 2012 values for temperatures unrecorded prior to weather station setup). The dashed black line is the 1-D thermal model of equation (D7). The dashed green line is from the 2-D model in Figure 7. Middle: three panes show RH (or water activity, green line), with inflexion around 17 December. Vertical blue lines are proportional to rainfall quoted in Table 1. The blue line and green circles are, respectively, instantaneous and monthly averaged relative humidity. Bottom: two panes separated by a whole year show daily burial depth inferred from peak temperature time lags after solar noon.

[41] Finally, for near-surface depths, we developed the simpler analytical 1-D model of equation (D7). As Figures 7 and 8 show, both models agreed well with measurements. For example, by properly accounting for dune mobility and variations in surface radiation and convection, they correctly predicted a lag of 70 days between the minimum monthly averaged ambient temperature in January and the corresponding minimum value later registered by probe 1 in March. As mentioned in section 2, because the dune moves at a similar rate than the thermal diffusion speed, ignoring dune advection would have instead produced erroneous predictions of its deep temperature field.

[42] As Figure 9 shows with probe 2, predictions from the 1-D models in mid-2012 reveal dissimilarities in insolation and convection between the leeward and windward faces. As quantified in Appendix D, higher insolation and lower convection both contribute to raising the temperature on the leeward face above the corresponding value on the windward slope. Because the 1-D model extrapolates surface temperature to the interior, it does not perform well deep within the dune, where temperature is equally affected by all nearby free surfaces. However, a 2-D model similar to Figsures 7 and 8 should lie between the two 1-D predictions and therefore capture buried temperature data more accurately.

[43] Figures 8 and 9 summarize buried probe observations. In Figure 8, the top panes show the temperature history of probe 1 (red line and symbols), a fit of mean diurnal ambient temperature (dashed blue line), and when the probe was close enough to the surface, times of sunrises and sunsets. Because our weather station did not operate before November 2011, we assumed that ambient temperatures were periodic annually, conforming to equation (C1), so that records in 2012 could be substituted for earlier times (triangles).

[44] The bottom two panes of Figure 8 show probe distance to the nearest free surface inferred using peak temperature lags from solar noon (equation 6). As expected from the steeper slope of the avalanche face (Figure 1), burial was faster than emergence. As Figure 6 shows, these inferred depths agree well with those calculated from the dune profile advancing at constant speed.

4.3. Moisture

[45] The middle three panes in Figures 8 and 9 show deep moisture records, with superimposed precipitation from Table 1. We interpret these data by modeling sand desorption and wetting using the equation of *Richards* [1931]

$$\frac{\partial \theta}{\partial t} = \nabla \cdot \left[\frac{K}{\mu_w} (\rho_w g \hat{\mathbf{z}} - \frac{\partial \Psi}{\partial \theta} \nabla \theta) \right], \tag{8}$$

which governs the evolution of the water volume fraction $\theta \simeq \rho_s \Omega / \rho_w$ in a porous sand of solid volume fraction ν, material density ρ_m, and bulk density $\rho_s = \nu \rho_m$. In equation (8), μ_w and density ρ_w are, respectively, the dynamic viscosity and density of liquid water; g is gravitational acceleration, $\hat{\mathbf{z}}$ is the upward vertical unit vector, $\Psi > 0$ is capillary suction pressure, and K is the unsaturated permeability at θ. Although sand, like any soil with a distribution of pore size, exhibits a hysteretic water retention

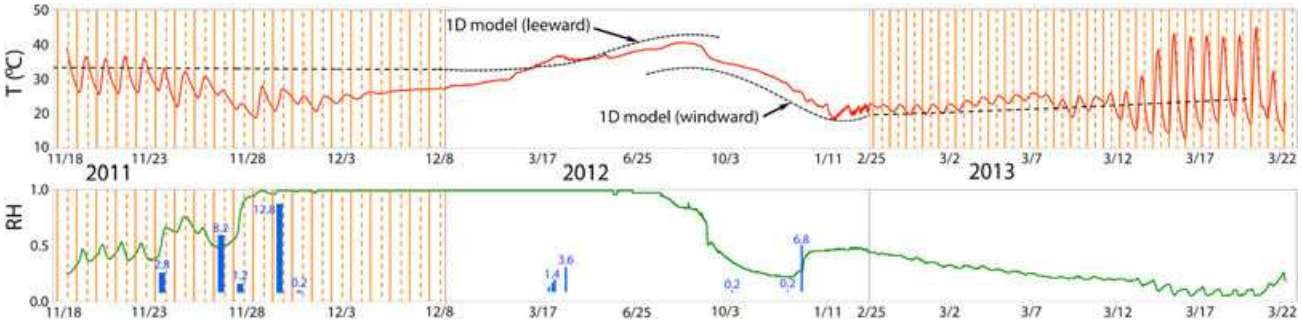

Figure 9. Data from probe 2. Lines, see Figure 8. Top: buried temperature versus time from November 2011 to March 2013 with magnified timescales during burial and emergence phases. The 1-D models are based upon the respective leeward and windward surface temperatures calculated in Appendix D. Bottom: relative humidity and rain records.

curve [*Mualem and Miller*, 1979; *Parlange*, 1980; *van Genuchten and Nielsen*, 1985; *Kool and Parker*, 1987; *Huang et al.*, 2005], desorption from saturation at $\theta = 1 - \nu$ has a limiting behavior that is conveniently modeled as $\theta = (1 - \nu)$ for $\Psi < \Psi_a$ and

$$\theta = (1 - \nu)(\Psi_a/\Psi)^{1/b} \tag{9}$$

otherwise [*Bittelli et al.*, 2008], where Ψ_a is the "air entry potential", i.e., the suction pressure one must exceed to force air into the saturated porous medium. Although the initial water volume fraction is generally $< 1 - \nu$ after desert rains, we adopt the formulation of equation (9) to derive simple analytical expressions for desorption of our sands. First, to estimate the unsaturated permeability K, we substitute it in the heuristic correction of *Brooks and Corey* [1964]

$$K = K_0 \left(\frac{\theta}{1-\nu}\right)^2 \frac{\int_{\theta'=0}^{\theta} d\theta'/\Psi^2}{\int_{\theta'=0}^{1-\nu} d\theta'/\Psi^2} = K_0 \left(\frac{\theta}{1-\nu}\right)^{2b+3}, \tag{10}$$

where K_0 is the saturated sand permeability. In this case, equation (8) may be written

$$\frac{\partial \theta}{\partial t} + \mathbf{u}_{\text{eff}} \cdot \nabla\theta = \nabla \cdot (D_{\text{eff}} \nabla\theta), \tag{11}$$

with effective nonlinear advection velocity

$$\mathbf{u}_{\text{eff}} = -\left[\frac{\rho_w g K_0}{\mu_w (1-\nu)}\right] (3 + 2b) \left(\frac{\theta}{1-\nu}\right)^{2b+2} \hat{\mathbf{z}}. \tag{12}$$

and diffusion coefficient

$$D_{\text{eff}} = \left[\frac{\psi_a K_0}{\mu_w (1-\nu)}\right] b \left(\frac{\theta}{1-\nu}\right)^{b+2}, \tag{13}$$

leading to a local Péclet number $u_{\text{eff}}\sqrt{K}/D_{\text{eff}} = (\rho_w g\sqrt{K_0}/\Psi_a)[(3+2b)/b][\theta/(1-\nu)]^{(3+2b)/2}$ sharply decreasing with θ. Therefore, because θ quickly falls as rain permeates the porous surface, diffusion controls desorption over long times. (This phenomenon is similar to the wetting of porous soils, where diffusion dominates advection at low θ, implying shallow water penetration. Conversely, at high θ near saturation, advection prevails).

[46] To obtain analytical predictions for long-term moisture desorption, we assume that rain is initially accumulated at a uniform volume fraction over a thin layer, that evaporation or advection are negligible, and that the RH probe remains buried at the center of this region. Then, as Appendix F ("Water Desorption") shows , the solution of equation (11) is

$$\theta_p = (1 - \nu)\left[\frac{h_R^2 \mu_w}{(1-\nu) 4\pi t \Psi_a K_0 b}\right]^{\frac{1}{4+b}}, \tag{14}$$

which decays rapidly at first but then much more slowly. After rains of $h_R \simeq 27.2$ mm fell in November 2011, equation (14) predicts that it would take $\simeq 240$ days to desorb sands down to $\Omega = 1\%$. This predicted duration is on

Table 1. Pluviometric Record h_R (mm) and Significant Events[a]

Date	h_R (mm)	Comments
January 2011	18.8	monthly aggregate
February 2011	1.8	monthly aggregate
March 19–21, 2011	0	near-surface diurnal measurements
April 12, 2011	2.4	
April 13, 2011	2.2	
April 14, 2011	0.6	
April 15, 2011	1.0	2 weeks before probe 1 disappeared
May 1, 2011	0	probe 1 disappears in nearly dry sand
November 7, 2011	1.8	
November 9, 2011	0.2	
November 18, 2011	0	probe 2 is buried
November 23, 2011	2.8	moisture rises around probe 2
November 26, 2011	8.2	
November 27, 2011	1.2	
November 28, 2011	0	probe 2 reaches RH $\simeq 1$
November 29, 2011	12.8	
November 30, 2011	0.2	
December 5–17, 2011	0	probe 1 at $x \simeq 2.8$ m feels November rains
March 26, 2012	0.8	
March 30, 2012	1.4	
March 31, 2012	0.2	
April 1, 2012	1.8	
April 2, 2012	0.4	
April 13, 2012	3.6	
June 21, 2012	0	RH at probe 2 becomes < 1
July 6, 2012	0	probe 1 surfaces
October 4, 2012	0.2	
December 1, 2012	0.2	
December 16, 2012	6.8	probe 2 at $x \simeq 0.6$ m
March 17–22, 2013		emergence of probe 2

[a] x is probe depth.

the order of the 200 day plateau at high water activity that "probe 2" experienced.

[47] To describe the wetting of initially dry sands, we deduce its limiting retention curve from equation (9) using the heuristic construction that *Parlange* [1976] proposed. As outlined in Appendix G ("Wetting"), we then calculate the time t_p required for rainwater to penetrate a dry dune to the depth x_p,

$$t_p = \left[\frac{(2-b)\mu_w(1-\nu)x_p}{(4+b)(3+2b)\rho_w g K_0}\right]^{\frac{4+b}{2-b}} \left[\frac{(1-\nu)4\pi\Psi_w K_0 b}{h_R^2\mu_w}\right]^{\frac{2+2b}{2-b}}. \quad (15)$$

[48] Combining with equation (14), we then estimate the peak water volume fraction at that depth,

$$\theta_p \simeq (1-\nu)\left[1+\frac{1}{b}\right]^{\frac{b(2+2b)}{(2-b)(4+b)}} \left[\frac{(4+b)(3+2b)h_R^2\rho_w g}{(2-b)(1-\nu)^2 4\pi b x_p \Psi_a}\right]^{\frac{1}{2-b}}. \quad (16)$$

[49] These equations imply that it only took 12 days for the November 2011 rains with cumulative $h_R \simeq 27.2$ mm to reach "probe 1" buried down to $x_p \simeq 2.8$ m. This prediction has the right order of magnitude: Following the last major rainfall on 29 November, "probe 1" recorded a noticeable downward temperature inflection 6 days later, and humidity visibly edged upward another 12 days afterward (green arrow in Figure 8). Equations (15) and (16) also show that substantial water can quickly sink to the depth $x_J = \sqrt{\alpha_s J/\pi}$ below which harsh diurnal temperature variations are inconsequential. For example, they predict that the 12.8 mm rain falling on 29 November reached $x_J \simeq 10$ cm at the volume fraction $\theta_p \simeq 0.11$ in a mere 28 min.

[50] In short, the data support four principal conclusions. First, humidity around deep sand grains crucially depends on whether or not precipitation occurred when those grains were trapped below the leeward avalanche face. As Figures 8 and 9 show, probe 1 finally disappeared below the surface 2 weeks after the last major rain, thus allowing sands to dry up around it. In contrast, because probe 2 was sunk just ahead of major precipitation, it recorded elevated relative humidity for 8 months.

[51] Second, as probe 1 recorded shortly after precipitations in November 2011, some rain moisture quickly reaches depths at which it was sheltered from harsh diurnal ambient variations. Equations (15) and (16) capture this behavior by modeling water penetration.

[52] Third, as probe 2 reveals, rainwater initially adsorbed on leeward-trapped sands can maintain high relative humidity nearby for a long time. As equation (13) suggests, this is because the effective diffusion of liquid water decreases as a power > 2 of volumetric water content θ, and thus keeps on slowing down during water desorption. This deep sustainability of rain moisture, which follows rapid water drainage and aeolian deposition of dry sands leeward, explains why *Louge et al.* [2010] had observed more humid sands below the windward surface than near the crest of a mobile barchan dune in the Sahara.

[53] Fourth, deep moisture emerging on the windward slope gradually dries up as it approaches the surface. There, variations in relative humidity become tied instead to a diurnal cycle similar to the one in Figure 4. Thus, although morning dew might still produce a relatively high relative humidity affecting surface cohesion, such an effect remains ephemeral.

5. Microbiological Implications

[54] To gauge whether sufficient moisture is available for microorganism survival, microbiologists invoke the "activity" a_w of a water solution, which at equilibrium is equal to the relative humidity of the surrounding moist air, a_w = RH [*Grant*, 2004]. To compete for water against nearby hydrophilic minerals, live microbes typically require $a_w \gtrsim 0.7$ [*Mugnier and Jung*, 1985], unless they are "xerophiles" that can withstand extreme desiccation [*Beblo et al.*, 2009; *Ponizovskaya et al.*, 2011].

[55] Adopting this benchmark, we identify regions within the sand dune where the threshold is reached. First, we note that Figure 8 and 9 paint very different pictures of deep habitat around the two buried probes. Because probe 1 disappeared below the surface at a time when the surrounding sands were dry, it experienced a relative humidity less than what *Mugnier and Jung* [1985] consider necessary to support microbes, except in the period from 28 March to 1 June 2012, when moisture gradually rose following deep penetration of rain water in November 2011. In contrast, because probe 2 was sunk just ahead of major precipitation, it recorded elevated water activity for 8 months in a range known to sustain microbial life. Crucially, once either probe reached a depth $\sim$ 20 cm where diurnal temperature variations disappear, temperature remained relatively mild throughout deep burial. This suggests that moisture alone governs microbial viability deep in the dune.

[56] The data also implies that moisture is trapped locally, rather than distributed uniformly. As equations (12)–(16) showed, because effective advection and diffusion of liquid water slow down with decreasing volume fraction, a small amount of rain moisture can endure for several months near the buried sands that collected it. In fast-moving mobile dunes, much of the moisture deposited by rain on the windward slope can be lost to aeolian drying and erosion. In contrast, moist sands trapped below the leeward avalanche face behave like probe 2, remaining humid until they emerge upwind. Therefore, individual regions within a relatively fast moving mobile dune can possess (or not possess) sufficient moisture for microbial activity, depending on whether or not rain fell on the avalanche face months earlier. If they do, then moisture can persist much longer than typical microbial incubation times. As sands approach the surface, rain falling overhead can also add to their moisture. However, by and large, deep sands "remember" whether or not precipitation fell as they were trapped on the leeward avalanche.

[57] Meanwhile, diurnal data from the near-surface instruments of section 3 confirmed that temperature is mild, steady, and invariant at depths $x \gtrsim 20$ cm, while humidity remains nearly constant. As Figure 4 showed, diurnal humidity variations were limited to depths $x \lesssim 5$ cm. Water activity then gradually increased with x, reaching a level conducive to microbial survival for $x > 11$ cm.

[58] Using the live stain technique of *Gommeaux et al.* [2010], we confirmed that microbes were present on sand grains sampled below the upwind slope of the same dune (Figure 10). There, we also found evidence of biological respiration by collecting gas samples at depths of 30, 60, and 90 cm in April 2012. To that end, we used a AMS gas vapor-sampling kit connecting a conical tip via a teflon tube to a brass fitting hermetically holding a septum stopper. We

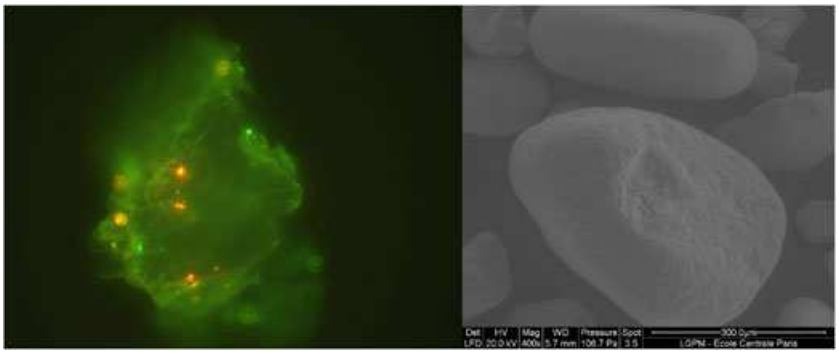

Figure 10. Microbial life on a Qatar dune sand grain. Left: Fluorescence micrograph of a single sand grain showing an abundance of bacteria. Live cells stained green with Syto 9 using a technique similar to *Gommeaux et al.* [2010]. Cells stained red/orange with propidium iodide are dead or dormant (400X magnification using a Zeiss Axio LSM 710 Fluorescence Microscope). Right: image of a similar sand grain from an FEI Quanta 200 Environmental Scanning Electron Microscope (ESEM) in low vacuum mode. We report particle size distribution in Appendix E ("Dunes, Sand Size, and Mass").

withdrew dune gases through the septum using a syringe needle and after quickly purging possible air contaminants, injected a sample by piercing the rubber septum of a vacutainer, slightly pressurizing the latter, so no gas could contaminate its contents during travel to Cornell's Stable Isotope Laboratory. There, a Thermo Delta V isotope ratio mass spectrometer interfaced to a "Gas Bench II" analyzer compared their stable isotope molar ratio $\Gamma \equiv {}^{13}CO_2/{}^{12}CO_2$ against the same ratio Γ_0 in the Vienna peedee belemnite standard [*O'Leary*, 1988]. Because respiration typically discriminates against $^{13}CO_2$, its resulting $\delta^{13}C \equiv (\Gamma/\Gamma_0) - 1$ is smaller than in CO_2 from abiotic origins.

[59] First, we noted that the CO_2 mole fractions 511 $\pm$ 25 ppm in the 17 samples collected were larger than the atmospheric value 391 $\pm$ 4 ppm. Then, we found that their $\delta^{13}C = -12 \pm 1‰$ was not only under the value of $\delta^{13}C \simeq -8‰$ in atmospheric CO_2, but it was also well below observations of $\delta^{13}C = +2 \pm 1‰$ from carbonates present in the same dry sand. (We found no significant variations in the mole fractions or the $\delta^{13}C$ of CO_2 with depth > 30 cm.) Therefore, CO_2 collected below the surface was partially of biological origin, adding further evidence to the microscopic observations in Figure 10.

[60] Finally, we frequently spotted on several mobile dunes, the "sand fish" *Scincus mitranus* seeking shelter by burrowing through the softer avalanche face [*Al-Johany et al.*, 1999], as well as insects like the desert beetles *Pimelia arabica* and *Adesmia cancellata*. These encounters suggested that hyperarid mobile dunes also offer a hospitable habitat to creatures other than microbes.

6. Conclusions

[61] Toward determining whether the protected core of hyperarid mobile sands presents a habitat with the potential to support microbes, we reported measurements of temperature and moisture below the surface of a barchan dune in Qatar on two widely different timescales and depths.

[62] On a diurnal period, strong variations in radiative and convective thermal fluxes were attenuated within the first 10 cm from the surface. Despite hyperarid ambient conditions, we observed in March 2011 that relative humidity at depths $\gtrsim$ 11 cm exceeded 0.7, a threshold above which microbiological development is possible [*Mugnier and Jung*, 1985]. In fact, based on recorded CO_2 mole fraction and carbon isotope ratios, we found that respiration occurred below the surface and was partially of biotic origin, confirming our detection of microbes on collected sand grains.

[63] We then measured humidity and temperature at greater depths using probes initially inserted through the leeward avalanche face, gradually overcome by the mobile dune and emerging windward 15 months later. Treating dune motion as a uniform advection superimposed on thermal diffusion, our analysis showed that deep temperature is predictable from wind statistics, crucially depends on dune speed, and lags stronger ambient seasonal variations. Deep temperatures were also mild and stable, suggesting that microbial viability at depths > 10 cm is governed by moisture alone.

[64] With these self-buried autonomous probes, we observed that deep moisture was largely determined by random precipitation that had occurred months earlier on the leeward avalanche face. Our analysis then showed why such moisture could endure on sand grains, until the latter finally emerged on the windward slope. Therefore, unlike temperature, moisture deep within a mobile dune depends too strongly on random rains to be predictable ahead of time. Dune mobility gives rise to the apparent travel of this moisture windward, creating a complex patchwork of diverse humidity levels below the upwind slope. Because deep moisture dries up as it resurfaces windward, relative humidity within 5 cm of the surface follows diurnal ambient variations. At dawn, our records of March 2011 suggested that it might reach sufficient levels to affect sand cohesion temporarily.

[65] We showed that hyperarid barchans conceal regions of moderate temperature and sufficient humidity allowing microbes to exist. Judging from the importance of biological soil crusts in limiting soil erosion [*Bowker et al.*, 2008], one wonders whether some of these microbes could be harnessed to fix the surface of mobile dunes.

[66] **Acknowledgments.** We are grateful to Sara Abdul-Majid for interrogating the buried probes, organizing logistics, and taking microscopic images; to Christopher Ogden for helping with field experiments; to Patrick Chasle for designing multiplexers for the temperature and capacitance instruments; to Matthew Blair for programming the data acquisition system; to Michel Babany for analyzing wind and ambient temperature data; to Anya Golkowski, M.-Jocelyn Comte, Xavier Lapert, and Floran Pierre for recording water adsorption; to Kimberlee and Jed Sparks for measuring stable carbon isotope ratios; to Rajesh Khiamal for recording sand permeability; to Nathalie Ruscassier for taking ESEM pictures of sand grains; to Robert Schindelbeck for establishing the water desorption curve; to Jean-Luc Métayer and Jean-Yves Brossault for measuring particle size distribution; to Patrick Perré, Jean-Yves Parlange, Tammo Steenhuis, Marco Bittelli, Dani Or, Simon Berkowicz, Shmuel Assouline, and Abraham Stroock for illuminating discussions on the drying of porous media; to Zellman Warhaft for discussing the atmospheric boundary layer; to Jean Taine for insight on radiation in porous media; to Theis Solling, Kristian Mogensen, and Steffen Bach for determining mineral composition with QEMScan; to Mohammad Al Sulaiti for supplying precipitation data; to Aurora Castilla for sharing her zoological expertise; and to Alexander Densmore and anonymous reviewers for their careful reading of the manuscript and valuable suggestions. This paper was made possible by the support of NPRP grant 09-546-2-206 from the Qatar National Research Fund. The statements made herein are solely the responsibility of the authors.

References

Al-Johany, A. M., M. K. Al-Sadoon, and S. A. Al-Farraj (1999), Thermal ecology and activity of the sand fish lizard Scincus mitranus (Scincidae) in Central Arabia, *J. King Saud Univ. Sci.*, *11*, 1–16.

Andreotti, B., P. Claudin, and S. Douady (2002), Selection of dune shapes and velocities. Part 1: Dynamics of sand, wind and barchans, *Eur. Phys. J. B*, *28*, 321–339.

Beblo, K., E. Rabbow, R. Rachel, H. Huber, and P. Rettberg (2009), Tolerance of thermophilic and hyperthermophilic microorganisms to desiccation, *Extremophiles*, *13*, 521–531.

Bagnold, R. (1935), The movement of desert sand, *Geog. J.*, *85*, 342–365.

Belnap, J. (2005), Crusts: Biological, in *Encyclopedia of Soils in the Environment*, edited by D. Hillel et al., pp. 339–347, Elsevier Ltd., Oxford, U. K.

Ben-Dor, E., N. Levin, A. Singer, A. Karnieli, O. Braun, and G. J. Kidron (2006), Quantitative mapping of the soil rubification process on sand dunes using an airborne hyperspectral sensor, *Geoderma*, *131*, 1–21.

Bittelli, M., F. Ventura, G. S. Campbell, R. L. Snyder, F. Gallegati, and P. Rossi Pisa (2008), Coupling of heat, water vapor, and liquid water fluxes to compute evaporation in bare soils, *J. Hydrol.*, *362*, 191–205.

Bokhary, H. A. (1998), Mycoflora of desert sand dunes of Riyahd region, Saudi Arabia, *J. King Saud Univ. Sci.*, *10*, 15–29.

Bowker, M. A., J. Belnap, V. B. Chaudhary, and N. C. Johnson (2008), Revisiting classic water erosion models in drylands: The strong impact of biological soils crusts, *Soil Biol. Chem.*, *40*, 2309–2316.

Bristow, C., S. Bailey, and N. Lancaster (2000), The sedimentary structure of linear sand dunes, *Nature*, *406*, 56–59.

Brooks, R. H., and A. T. Corey (1964), Hydraulic Properties of Porous Media, *Colorado State University Hydrology Paper*, *27*(3).

Carslaw, H. S., and J. C. Jaeger (1959), *Conduction of Heat in Solids*, 2nd ed., pp. 54–65, Clarendon Press, Oxford.

Charru, F., B. Andreotti, and P. Claudin (2013), Sand ripples and dunes, *Annu. Rev. Fluid Mech.*, *45*, 469–93.

Chen, S. X. (2008), Thermal conductivity of sands, *Heat Mass Transfer*, *44*, 1241–1246.

de Félice, P. (1968), Etude des échanges de chaleur entre l'air et le sol sur deux sols de nature différente, *Geophys. Bioklimatol. Ser. A*, *16*, 70–80.

Durán, O., and H. Herrmann (2006), Vegetation against dune mobility, *Phys. Rev. Lett.*, *97*, 188001.

Fang, H. Y., Q. G. Cai, H. Chen, and Q. Y. Li (2007), Mechanism of formation of physical soil crust in desert soils treated with straw checkerboards, *Soil Tillage Res.*, *93*, 222–230.

Forster, S. M. (1979), Microbial aggregation of sand in an embryo dune system, *Soil Biol. Biochem.*, *11*, 537–543.

Forster, S. M., and T. H. Nicolson (1981), Aggregation of sand from a maritime embryo sand dune by microorganisms and higher plants, *Soil Biol. Biochem.*, *13*, 199–203.

Frank, X., and P. Perré (2012), Droplet spreading on a porous surface: A lattice Boltzmann study, *Phys. Fluids*, *24*, 042101, doi:10.1063/1.3701996.

Fraysse, N., H. Thomé, and L. Petit (1999), Humidity effects on the stability of a sandpile, *Eur. Phys. J. B*, *11*, 615–619.

Gommeaux, M., M. Barakat, G. Montagnac, R. Christen, F. Guyot, and T. Heulin (2010), Mineral and bacterial diversities of desert sand grains from South-East Morocco, *Geomicrobiol. J.*, *27*, 76–92, doi:10.1080/01490450903393066.

Grant, W. D. (2004), Life at low water activity, *Philos. Trans. R. Soc. London, Ser. B.*, *359*, 249–267, doi:10.1098/rstb.2004.1502.

Gray, J. M. N. T., and K. Hutter (1997), Pattern formation in granular avalanches, *Continuum Mech. Thermodyn.*, *9*, 341–345.

Hersen, P. (2004), On the crescentic shape of barchan dunes, *Eur. Phys. J. B*, *37*, 507–514.

Hersen, P., K. H. Andersen, H. Elbelrhiti, B. Andreotti, P. Claudin, and S. Douady (2004), Corridors of barchan dunes: Stability and size selection, *Phys. Rev. E*, *69*, 011304.

Heulin, T., M. Barakat, R. Christen, M. Lesourd, L. Sutra, G. De Luca, and W. Achouak (2003), *Ramlibacter tataouinensis* gen. nov., sp. nov., and *Ramlibacter henchirensis* sp. nov., cyst-producing bacteria isolated from subdesert soil in Tunisia, *Int. J. Syst. Evol. Microbiol.*, *53*, 589–594.

Heulin, T., G. De Luca, M. Barakat, A. de Groot, L. Blanchard, P. Ortet, and W. Achouak (2012), Bacterial adaptation to hot and dry deserts, in *Adaptation of Microbial Life to Environmental Extremes*, edited by H. Stan-Lotter et al., pp. 69–85, Springer-Verlag, Wien.

Ho, T. D., A. Valance, P. Dupont, and A. Ould El-Moctar (2011), Scaling laws in aeolian sand transport, *Phys. Rev. Lett.*, *106*, 094501.

Hu, C., Y. Liu, L. Song, and D. Zhang (2002), Effect of desert soil algae on the stabilization of fine sands, *J. Appl. Phycol.*, *14*, 281–292.

Hu, C., Y. Liu, B. S. Paulsen, D. Petersen, and D. Klaveness (2003), Extracellular carbohydrate polymers from five desert soil algae with different cohesion in the stabilization of fine sand grain, *Carbohydr. Polym.*, *54*, 33–42.

Huang, H.-C., Y.-C. Tan, C.-W. Liu, and C.-H. Chen (2005), A novel hysteresis model in unsaturated soil, *Hydrol. Processes*, *19*, 1653–1665.

Iwamatsu, M., and K. Horii (1996), Capillary condensation and adhesion of two wetter surfaces, *J. Colloid Interface Sci.*, *182*, 400–406.

Katata, G., H. Nagai, H. Ueda, N. Agam, and P. R. Berliner (2007), Development of a land surface model including evaporation and adsorption processes in the soil for the land-air exchange in arid regions, *J. HydroMet.*, *8*, 1307–1324.

Kidron, G. J., I. Herrnstadt, and E. Barzilay (2002), The role of dew as a moisture source for sand microbiotic crusts in the Negev Desert, Israel, *J. Arid. Environ.*, *52*, 517–533, doi:10.1006/jare.2002.1014.

Kobayashi, T., A. Matsuda, M. Kamichika, and T. Sato (1986), Studies of the dry surface layer in a sand dune field. 1: Modeling of the dry surface layer of sand under isothermal steady conditions, *J. Agr. Met.*, *42*, 113–118.

Kobayashi, T., A. Matsuda, M. Kamichika, and Y. Yamamura (1991), Why the thickness of the dry surface layer in sand dune fields exhibits a diurnal variation?, *J. Agr. Met.*, *47*, 3–9.

Kool, J. B., and J. C. Parker (1987), Development and evaluation of closed-form expressions for hysteretic soil hydraulic properties, *Water Resour. Res.*, *23*, 105–114.

Levin, N., G. J. Kidron, and E. Ben-Dor (2007), Surface properties of stabilizing coastal dunes: Combining spectral and field analyses, *Sedimentology*, *54*, 771–788.

Livingstone, I., G. F. Wiggs, and C. M. Weaver (2007), Geomorphology of desert sand dunes: A review of recent progress, *Earth Sci. Rev.*, *80*, 239–257.

Louge, M. Y., A. Valance, H. Mint Babah, J.-C. Moreau-Trouvé, A. Ould el-Moctar, and D. Ould Ahmedou (2010), Seepage-induced penetration of humidity and dust beneath ripples and dunes, *J. Geophys. Res.*, *115*, F02002, doi:10.1029/2009JF001385.

Mason, T. G., A. J. Levine, D. Ertaş, and T. C. Halsey (1999), Critical angle of wet sandpiles, *Phys. Rev. E*, *60*, R5044–R5047.

McKee, E. D. (Ed.) (1979), *A Study of Global Sand Seas*, Geological Survey Professional Paper 1052, US Department of the Interior and NASA, United States Government Printing Office, Washington, D. C.

Mitarai, N., and F. Nori (2006), Wet granular materials, *Adv. Phys.*, *55*, 1–45.

Mualem, Y., and E. E. Miller (1979), A hysteresis model based on an explicit domain-dependence function, *Soil Sci. Soc. Am. J.*, *43*, 1067–1073.

Mugnier, J., and G. Jung (1985), Survival of Bacteria and Fungi in relation to water activity and the solvent properties of water in biopolymer gels, *Appl. Environ. Microbiol.*, *50*, 108–114.

O'Leary, M. H. (1988), Carbon isotopes in photosynthesis, *BioScience*, *38*, 328–336.

Ould Ahmedou, D., A. Ould Mahfoudh, P. Dupont, A. Ould el-Moctar, A. Valance, and K. R. Rasmussen (2007), Barchan dune mobility in Mauritania related to dune and interdune sand fluxes, *J. Geophys. Res.*, *112*, F02016, doi:10.1029/2006JF000500.

Parlange, J.-Y. (1976), Capillary hysteresis and the relationship between drying and wetting curves, *Water Resour. Res.*, *12*, 224–228.

Parlange, J.-Y. (1980), Water transport in soils, *Ann. Rev. Fluid Mech.*, *12*, 77–102.

Ponizovskaya, V. B., A. B. Antropova, V. L. Mokeeva, E. N. Bilanenko, and L. N. Chekunova (2011), Effect of water activity and relative air humidity on the growth of *Penicillium chrysogenum* Thom, *Aspergillus repens* (Corda) Sacc., and *Trichoderma viride* Pers. isolated from living spaces, *Microbiology*, *80*, 378–385.

Rasmussen, K. R., J. D. Iversen, and P. Rautahemio (1996), Saltation and wind-flow interaction in a variable slope wind tunnel, *Geomorphology*, *17*, 19–28.

Ravi, S., T. M. Zobeck, T. M. Over, G. S. Okin, and P. D'Odorico (2006), On the effect of moisture bonding forces in air-dry soils on threshold friction velocity of wind erosion, *Sedimentology*, *53*, 597–609, doi:10.1111/j.1365-3091.2006.00775.x.

Requena, N., E. Perez-Solis, C. Azcón-Aguilar, P. Jeffries, and J.-M. Barea (2001), Management of indigenous plant-microbe symbioses aids restoration of desertified ecosystems, *Appl. Environ. Microbiol.*, *67*, 495–498.

Richards, L. A. (1931), Capillary conduction of liquids through porous mediums, PhD thesis, Cornell University.

Rotnicka, J. (2013), Aeolian vertical mass flux profiles above dry and moist sandy beach surfaces, *Geomorphology*, *187*, 27–37.

Sauermann, G., K. Kroy, and H. J. Herrmann (2001), Continuum saltation model for sand dunes, *Phys. Rev. E*, *64*, 031305.

Schwämmle, V., and H. Herrmann (2005), A model of barchan dunes including lateral shear stress, *Eur. Phys. J. E*, *16*, 57–65.

Shahraeeni, E., and D. Or (2010), Pore-scale analysis of evaporation and condensation dynamics in porous media, *Langmuir*, *26*, 13,924–13,936.

Shang, S., R. N. Horne, and H. J. Ramey (1995), Water vapor adsorption on geothermal reservoir rocks, *Geothermics*, *24*, 523–540.

Sterk, G. (2003), Causes, consequences and control of wind erosion in Sahelian Africa: A review, *Land Degrad. Dev.*, *14*, 95–108.

Stutz, J. C., R. Copeman, C. A. Martin, and J. B. Morton (2000), Patterns of species composition and distribution of arbuscular mycorrhizal fungi in arid regions of southwestern North America and Namibia, Africa, *Can. J. Bot.*, *78*, 237–245.

Taine, J., F. Bellet, V. Leroy, and E. Iacona (2010), Generalized radiative transfer equation for porous medium upscaling: Application to the radiative Fourier law, *Int. J. Heat Mass Transfer*, *53*, 4071–4081.

Tegzes, P., T. Vicsek, and P. Schiffer (2003), Development of correlations in the dynamics of wet granular avalanches, *Phys. Rev. E*, *67*, 051303-1–17.

Titus, J. H., P. J. Titus, R. S. Novak, and S. D. Smith (2002), Arbuscular mycorrhizae of Mojave desert plants, *Western North American Nat.*, *62*, 327–334.

van Genuchten, M. T., and D. R. Nielsen (1985), On describing and predicting the hydraulic properties of unsaturated soil, *Ann. Geophys.*, *3*, 615–627.

Vriend, N. M., M. L. Hunt, and R. W. Clayton (2012), Sedimentary structure of large sand dunes: Examples from Dumont and Eureka dunes, California, *Geophys. J. Int.*, *190*, 981–992.

Vriend, N. M., M. L. Hunt, R. W. Clayton, C. E. Brennen, K. S. Brantley, and A. Ruiz-Angulo (2007), Solving the mystery of booming sand dunes, *Geophys. Res. Lett.*, *34*, L16306, doi:10.1029/2007GL030276.

Wyngaard, J. C. (2010), *Turbulence in the Atmosphere*, Cambridge Univ. Press, N. Y., ISBN 978-0-521-88769-4.

Yizhaq, H., Y. Ashkenazy, and H. Tsoar (2007), Why do active and stabilized dunes coexist under the same climatic conditions?, *Phys. Rev. Lett.*, *98*, 188001.

Zhang, D., C. Narteau, and O. Rozier (2010), Morphodynamics of barchan and transverse dunes using a cellular automaton model, *J. Geophys. Res.*, *115*, F03041, doi:10.1029/2009JF001620.

Zhang, D., C. Narteau, O. Rozier, and S. Courrech du Pont (2012), Morphology and dynamics of star dunes from numerical modelling, *Nat. Geosci.*, *5*, 463–467, doi:10.1038/ngeo1503.